

# Surface Acoustic Wave action on Microfluidic Channels and Microparticles

Erin R. Dauson<sup>a</sup>, Kelvin B. Gregory<sup>a</sup>, David W. Greve<sup>b</sup>, Irving J. Oppenheim<sup>a</sup>

<sup>a</sup>Civil and Environmental Eng., Carnegie Mellon University, Pittsburgh, PA 15213

<sup>b</sup>Electrical and Computer Eng., Carnegie Mellon University, Pittsburgh, PA 15213

## ABSTRACT

We describe lithium niobate SAW devices and their wave structure at different resonant frequencies, and we discuss the difference between PDMS and PMMA as the material for the microfluidic channel. We discuss the different wave structure for SAW devices operating at different resonant frequencies, showing simulation results and laboratory measurements. We discuss our recent studies to sort microparticles by size.

**Keywords:** Microfluidics, microparticles, PDMS, PMMA, SAW device, standing waves.

## 1. INTRODUCTION

Particles can be concentrated in microfluidic devices using standing acoustic waves created by interdigitated transducers (IDTs) on piezoelectric substrates. The effectiveness and energy efficiency of this process however is subject to the wave types created, the ability of those waves to couple to channels on the substrate and to the fluid in the channels. It is useful therefore to evaluate both the type of waves created by our IDTs, and the channel materials we use in these devices.

## 2. BACKGROUND: ACOUSTIC MICROFLUIDIC DEVICES

Surface acoustic waves (SAWs) propagate on the surface of solids while bulk waves travel with higher velocities through the volume. Acoustic wave components at or near the surface of a substrate can be used to excite waves in microfluidic channels, and because the largest proportion of SAW energy is near the surface SAWs are desirable (efficient) for transferring energy into the fluid within a channel. We use interdigitated transducers (IDTs) to excite acoustic waves on the piezoelectric material lithium niobate. By exciting these waves from two different sides of a substrate or channel, we can create a field of standing waves.

Standing acoustic waves in a microfluidic channel create an acoustic potential field in the fluid in the channel. In an acoustic potential field, microparticles concentrate at nodes or antinodes of the standing waves, depending on the particle properties. The velocity at which particles migrate towards these nodes or antinodes is dependent on the particle volume, mass, density and stiffness. With appropriately controlled fields, therefore, these differences may be employed to separate different types of microparticles.

In our basic device design, a microfluidic channel is bonded parallel to and between two parallel IDTs. In prior work by Johansson et al.<sup>6</sup>, Shi et al.<sup>1</sup>, and others, channels have been made from Polydimethylsiloxane (PDMS) because this material can be easily fabricated into microfluidic channels using standard soft lithographic techniques. We, however, also fabricate channels out of poly (methyl methacrylate) (PMMA) as an alternative to PDMS. PMMA can be machined for easy fabrication and has less acoustic damping than PDMS, and if employed effectively it has the potential to create devices that transfer more of the energy into the fluid.

## 3. FABRICATION

### 3.1 IDT Fabrication

Pairs of interdigitated electrodes can be used to excite and detect waves on a lithium niobate crystal substrate because lithium niobate is piezoelectric, meaning it deforms when an electrical potential is applied and responds to deformation

by creating an electrical potential. We fabricated IDTs on 0.5 mm thick pieces of Y-cut, Z-propagating clear lithium niobate using a procedure described in detail in our previous work.<sup>2</sup> We fabricate IDT fingers with equal width and spacing, we use 20 electrode finger pairs for each IDT, and we overlap the fingers by a length of 8.1 mm. We fabricate the IDTs in pairs, separated in the propagation direction by 12 mm.

To fabricate IDTs we clean the substrate and then sputtering approximately 400  $\mu\text{m}$  of aluminum. We then use contact lithography and aluminum etch to define the IDT structures. We fabricated IDT pairs with 50  $\mu\text{m}$  finger width and spacing and with 25  $\mu\text{m}$  finger width and spacing, corresponding to 200  $\mu\text{m}$  and 100  $\mu\text{m}$  wavelengths, respectively. The manufacturer's specification for surface acoustic wave velocity on Y-cut, Z-propagating lithium niobate is 3488 m/s, so we expect a resonant frequency near 17.44 MHz for the 200  $\mu\text{m}$  wavelength devices and near 34.88 MHz for the 100  $\mu\text{m}$  wavelength devices. When excited with a sinusoidal voltage near the resonant frequency, the IDTs create waves in the piezoelectric substrate. By exciting both IDTs in a pair, or using an IDT or substrate edge as a reflective boundary, we can create standing waves in or on our substrate. In some experiments we apply a thick layer of photoresist between the IDT and the edge of the wafer to add damping to limit possible edge reflections. An example of these devices is shown in Figure 1.

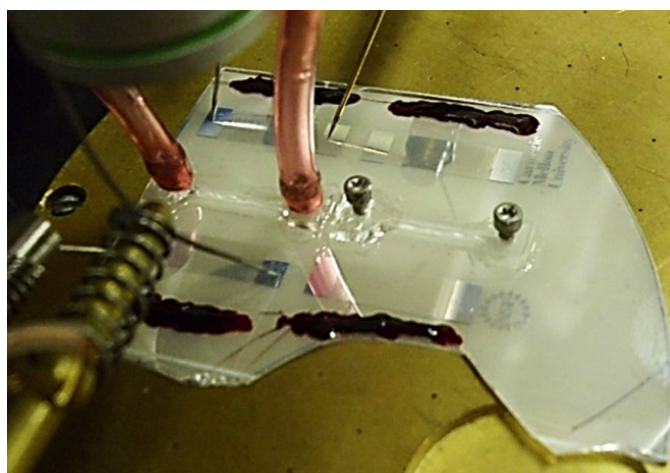


**Figure 1:** Devices on a piece of X-cut Y-Propagating lithium niobate. Two pairs of IDTs with PMMA channels bonded between each pair, and a damping layer applied between each IDT and the substrate edge. The channel on the right shows the aluminum screws used to interface with the channel, while the channel on the left demonstrates how those screws connect to the Tygon® tubing. The devices are mounted on a micromanipulator station with probes set on the left pair of IDTs for exciting the device.

### 3.2 PMMA Channels

In PMMA channel fabrication it is useful for channels to be sufficiently large for us to handle and place easily on the device, but (to reduce attenuation) we want to limit the distance the waves must travel through the PMMA. Therefore, using VisualMill we designed a PMMA channel with a height of 1.016 mm and a width (in the direction of wave propagation) of 2 mm, widening to 5 mm or 7 mm at the ends (outside of the path traveled by the waves) to make the channel easier to place and to enable fabricating the channel-world interface. The water channel is 254  $\mu\text{m}$  wide and between 75  $\mu\text{m}$  and 250  $\mu\text{m}$  deep. Figure 2 shows the simulated VisualMill cut of an example channel.

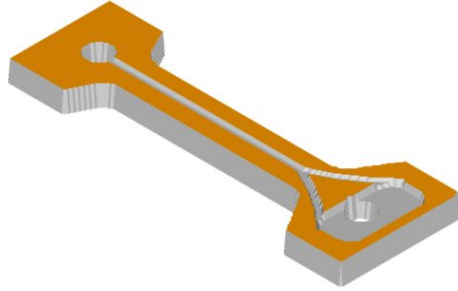


**Figure 2: Simulated PMMA channel, upside down and not yet bonded, to show the inlet holes for the world-channel interface and the y-shaped channel.**

At each end of the channel, a hole is drilled and then tapped for 0-80 screws. We use a 0.0295" drill bit to drill holes through the center of 0-80 x 3/32 Socket Head Cap Torx Screws. When the PMMA channel is attached to the SAW device, we can advance the aluminum screws into the holes, leaving space at the bottom of the hole for unrestricted flow. 3/16" Tygon® tubing slips over the socket head cap of the screw and can be easily attached or detached. To manufacture the channel we start with .040" thick Clear Cell Cast Acrylic Glass, and use a Minitech micromill and a 0.01" mill bit to machine the part of the channel through which the water flows. We then use the Minitech micromill and 0.0495" drill bit to drill the access holes to be tapped for screws, and a 0.05" mill bit to machine the outline and shape of the channel. We tap the holes by hand. Once the channels are fabricated we clean them using soap and water, rinse well with water, and then clean with methanol to remove any remaining residue or contaminants.

### **3.3 Bonding PMMA Channels to Lithium Niobate**

To bond the PMMA channel to the wafer we first clean the wafer using acetone followed by methanol. We then ash the SAW device in air for 5 minutes using a Harrick Plasma Cleaner. Next we use the plasma cleaner on both the wafer and the PMMA channel for 1 minute. This appears to temporarily increase the hydrophilicity of the PMMA channel, similar to the role of plasma ashing when attaching PDMS channels. We then place the channel at the appropriate location on the device substrate and heat the channel and wafer together for 25 minutes at 152°C before allowing it to cool for 10 minutes. Because lithium niobate is pyroelectric as well as piezoelectric, the heating process may generate a temporary voltage on the substrate, so it is helpful to discharge any voltage through grounding before proceeding.

The heating process softens the PMMA temporarily, and enables it to achieve closer contact with the substrate. In an adaptation of the method described in Langelier et al.<sup>3</sup> we apply Norland Optical Adhesive 61 in two small drops at either end of the channel at the interface between the channel and the substrate. Capillary pressure driven flow moves the epoxy into place between the substrate and the PMMA while avoiding the machined channel features because the abrupt change in hydraulic resistance at the edge of the channel features stops the capillary pressure driven flow.<sup>3</sup> Increasing the hydrophilicity of the PMMA using the plasma cleaner in air increases the wetting properties of the substrate and the PMMA channel, and consequently increases the flow rate from the capillary pressure driven flow. It is important to note that this increased hydrophilicity is temporary and decays, so extra time heating or cooling the substrate between the plasma cleaning and the application of epoxy affects the time and the effectiveness with which the epoxy spreads between the PMMA and the substrate.

After applying the epoxy we develop it under a fluorescent light for 12 hours to cure the epoxy. Because the channels are transparent, light from above reaches the epoxy, but the required exposure time is increased because of reduced UV transmission through PMMA. After curing we screw in the drilled aluminum screws, attach the Tygon® tubing and test the completed device.

## **4. WAVE TYPES AT OPERATING FREQUENCY**

Surface acoustic waves (SAWs) propagate at the surface of solids, with displacements that decay exponentially into the surface with a decay length of the order of the wavelength. Because SAWs have most of their energy concentrated near the surface, they can more effectively transfer energy to channels on the surface than bulk waves, and thus are preferred for efficient excitation of acoustic fields within channels. IDTs create surface waves on lithium niobate wafers in SAW filters and other common applications; however, at the low frequencies typically used for particle concentration, the

wavelengths are of the order of the substrate thickness. Accordingly, the waves generated may not be pure surface waves; indeed, plate (Lamb) waves are sometimes observed.

#### 4.1 Electrical measurements of IDTs on LiNbO<sub>3</sub> and wave reflections

IDT pairs were fabricated as described above with 200  $\mu\text{m}$  wavelength and 100  $\mu\text{m}$  wavelength on Y-cut, Z-propagating clear lithium niobate wafers, with damping photoresist applied outside of the active area of each IDT pair. We then electrically characterized the devices using a Rohde and Schwartz ZVB4 network analyzer, and recorded  $S_{11}$ , a scattering parameter that indicated the ratio of reflected wave amplitude to applied wave amplitude for the system, with the opposing IDT matched by the network analyzer with 50  $\Omega$  impedance. The network analyzer measured  $S_{11}$  over a frequency range around the resonant frequency, and then transformed the results into the time domain. As shown in Figure 3 the time domain gives us information about reflections by displaying peaks at times indicative of the round trip time for a wave at a particular velocity traveling from the exciting IDT to the reflective area and back. With an IDT wavelength of 200  $\mu\text{m}$ , the center to center distance between the IDT pairs is 16 mm. At a SAW velocity of 3488 m/s, we expect the round trip from an exciting IDT to an opposing IDT and back to require about 9.2  $\mu\text{s}$ . With an IDT wavelength of 100  $\mu\text{m}$ , the center to center distance between the two pairs of IDTs is 14 mm, and the expected round trip time is about 8.0  $\mu\text{s}$ . The graphs in Figure 3 for IDT pairs at 200  $\mu\text{m}$  and 100  $\mu\text{m}$  wavelengths (bare, before placing channels between the IDTs) agree well with these expectations by showing peaks near 9.2  $\mu\text{s}$  and 8.0  $\mu\text{s}$  respectively.

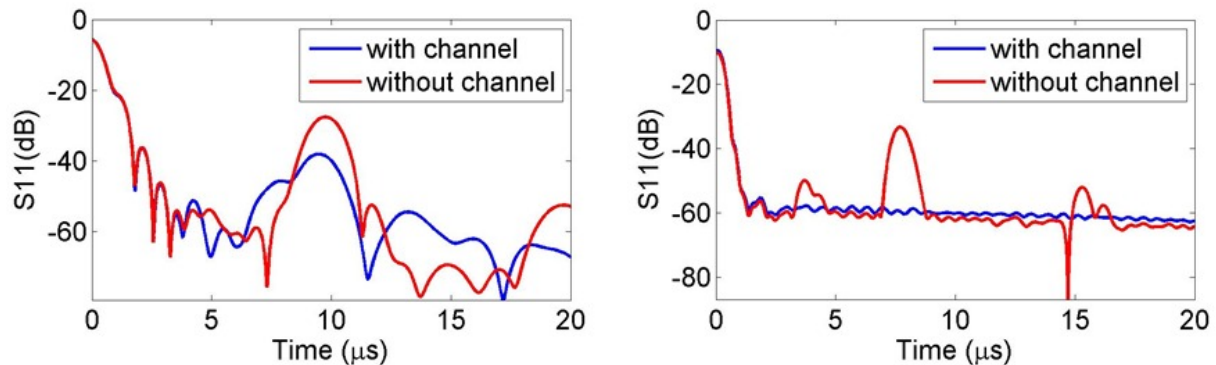


**Figure 3: Left graph: Time domain  $S_{11}$  measurements of a 200  $\mu\text{m}$  wavelength IDT on Y-cut, Z-propagating lithium niobate wafers with a 16 mm center to center distance to an opposing IDT, with and without a diagonal PMMA channel bonded between the two IDTs. Right graph: Time domain  $S_{11}$  measurements of a 100  $\mu\text{m}$  wavelength IDT on Y-cut, Z-propagating lithium niobate wafers with a 14mm center to center distance to an opposing IDT, with and without a diagonal PMMA channel bonded between the two IDTs.**

After electrically characterizing the two pairs of IDTs we bonded PMMA channels to the devices using the procedure described above, but instead of placing a channel parallel to the IDTs, we bonded the channels diagonally across the active area. As seen in Figure 3, after the addition of the channel, at the 200  $\mu\text{m}$  wavelength the amplitude of the peak at 9.2  $\mu\text{s}$  is decreased slightly, showing some energy transfer into the channel. At the 100  $\mu\text{m}$  wavelength, however, the peak at 8.0  $\mu\text{s}$  almost completely disappears. We hypothesize that the 100  $\mu\text{m}$ -wavelength waves (on a 500  $\mu\text{m}$  thick substrate) are much closer to true surface waves than the 200  $\mu\text{m}$ -wavelength waves. Since the largest displacements in the shorter wavelength waves are near the surface, more of that energy is transferred into the channel. In contrast, at the 200  $\mu\text{m}$  wavelength, much of the wave energy travels through the bulk of the material, and therefore can bypass the channel with less transfer of energy into the channel.

#### 4.1 Eigenmode analysis in COMSOL

To better understand the wave types appearing in our 0.5 mm thick substrate at these 200  $\mu\text{m}$  and 100  $\mu\text{m}$  wavelengths, we used COMSOL Multiphysics 4.3b to perform a 2D finite element eigenmode analysis. We simulated a piece of lithium niobate 0.5 mm thick and 200  $\mu\text{m}$  long with periodic boundary conditions on the two sides, and with the top and bottom surfaces free. We then identified surface wave-like modes with one and two wavelengths in the 200  $\mu\text{m}$  length of the model, corresponding to wavelengths of 200  $\mu\text{m}$  and 100  $\mu\text{m}$  respectively. Figure 4 shows four of these modes, with color representing vertical displacement. The eigenmodes with 100  $\mu\text{m}$  wavelength are very similar in appearance to surface waves that appear on a very thick substrate. (There are two distinct eigenmodes with nearly the same frequency which differ in the alignment of waves on the top and bottom surface.) Eigenmodes at 200  $\mu\text{m}$  wavelength show nearly

constant displacements through the entire substrate, approaching the appearance of S0 and A0 plate modes, and also displaying greater frequencysplitting. It is evident, especially at the 200 μm wavelength, that there are substantial displacements through the entire thickness of the substrate.

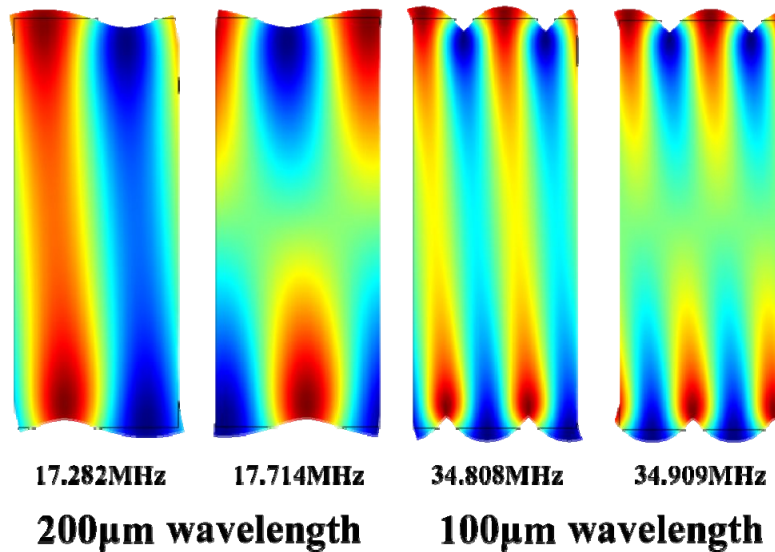


Figure 4: Eigenmodes, FEM model 200 μm long, 500 μm thick Y-cut, Z-propagating lithium niobate, free boundary conditions top and bottom, periodic boundary conditions left and right. Color represents vertical displacement in the Eigenmode.

#### 4.2 Wafer Simulation

To examine the wave types created by our IDTs, using COMSOL Multiphysics 4.3b we performed a 2D frequency domain finite element simulation of IDTs on a 0.5 mm thick piece of Y-cut, Z-propagating lithium niobate. To simplify the model to focus on wave types and wave behavior, we simulated a region 15 mm long, we modeled half of a 200 μm wavelength IDT at the left edge of the model (using a symmetry condition on that left boundary), and we modeled a complete (20 finger pair) IDT centered 13 mm from the left edge. We applied free boundary conditions to the top and bottom edges. To reduce the effect of reflection from the right boundary, we applied an absorbing boundary condition as suggested by Nielson<sup>4</sup> by applying boundary loads  $f_x$  and  $f_y$  at the edge given by  $f_x = -\rho c_p v_x$  and  $f_y = -\rho c_s v_y$  where  $c_p = 7288$  m/s is the longitudinal wave velocity,  $c_s = 3570$  m/s is the shear wave velocity,  $\rho$  is density,  $v_x$  and  $v_y$  are the velocities in the x and y directions, respectively.

In most cases we choose the damping parameters in the substrate by comparing the electrical response of the simulated IDTs to the measured electrical response of experimental IDTs. We choose a damping value that closely matches the shape for the peaks of the capacitance representing reflections near the resonant frequency.

We first performed a simulation with substrate damping chosen to attenuate the wave before reaching the right edge. Figure 5 shows the y displacement resulting when a wave is launched by the IDT with an excitation frequency of 16.25 MHz. The wave shape is similar to the eigenmodes discussed above and it is apparent that waves are not confined to the surface. It is important to note that this is not a consequence of mode conversion at the right edge, because the waves are attenuated before reaching that edge.

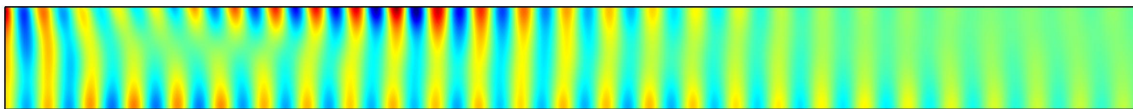


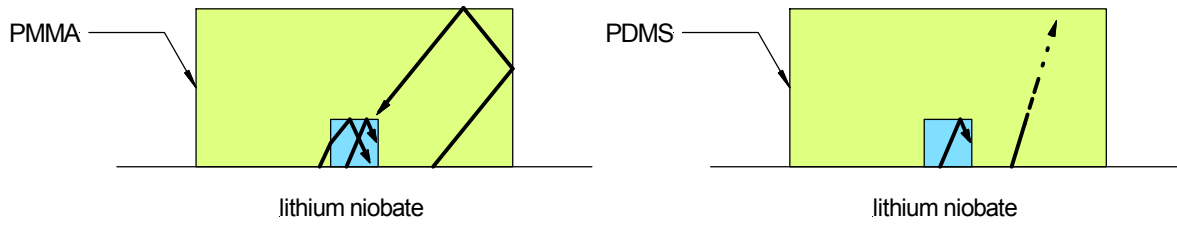
Figure 5: Frequency domain simulated 0.5 mm thick X-Y cut lithium niobate wafer with 200 μm wavelength half IDT at the left edge excited at 16.52 MHz. Color shows y component of displacement. Simulated damping is high so that waves do not reach the opposing end, and there is no opportunity for boundary mode conversion.

## 5. DIFFERENCE BETWEEN PMMA AND PDMS

PDMS is a soft material with a high Poisson ratio (near 0.495) which is acoustically similar to water, and, as discussed in our previous work<sup>5</sup> and by Langelier et al.,<sup>3</sup> causes high attenuation of waves traveling through it. Therefore, PDMS is not ideal for energy-efficient transfer of SAW energy into the water in the microfluidic channel. (PMMA, in contrast, causes less attenuation of waves, but is also a significantly harder material than PDMS.) Johansson et al. remark that with PDMS channels most of the acoustic energy entering the water comes from waves traveling in the substrate under the water, transferred directly from the substrate to the water.<sup>6</sup> Only a small portion of the acoustic energy in the water comes from longitudinal waves propagating through the PDMS.

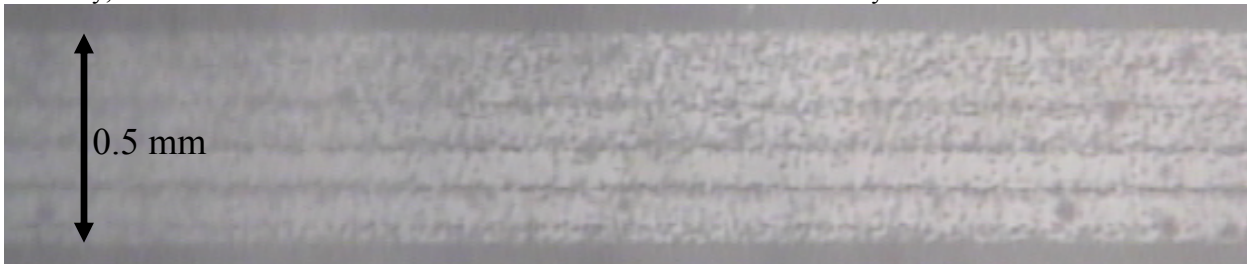
For applications of SAW device channels, PMMA differs from PDMS in a number of ways. Firstly, the longitudinal wave velocity in water (1480 m/s) is much closer to the longitudinal wave velocity in PDMS (~1020 m/s) than the longitudinal wave velocity in PMMA (2730 m/s). Because of the difference in wave velocities in different materials, at the interface between two different materials a traveling wave is deflected so that the wave fronts match at the boundaries but the wave directions differ. The angle (measured from the vertical) that a longitudinal wave (produced by the substrate surface wave interaction) will travel in the channel material and water, termed the Rayleigh angle, is therefore significantly lower in transmission from LiNbO<sub>3</sub> to PDMS (17.0°) than in transmission from LiNbO<sub>3</sub> to PMMA (51.5°).

Figure 6 contrasts the behavior of waves in PDMS and PMMA channels. In PDMS, the nodes and antinodes are primarily formed from waves emitted directly into the water channel. Waves emitted into the PDMS are strongly attenuated and are not important in forming nodes and antinodes in the water channel. In contrast, in PMMA, waves are emitted at an angle of about 51 degrees with respect to the normal. After reflection at channel surfaces, these waves can be transmitted into the water channel, resulting in additional nodes and antinodes beyond those formed by the directly emitted waves.



**Figure 6: Contrast of PMMA and PDMS showing possible wave paths**

This discussion is consistent with our experimental observations in PMMA and PDMS channels. Figure 7 shows the concentration of 6  $\mu\text{m}$  particles in a PDMS channel on 128° Y-cut black lithium niobate with a 200  $\mu\text{m}$  wavelength IDT pair driven at a frequency of 19.76 MHz. The fabrication of this particular device is described in a previous report.<sup>5</sup> In the image the concentrated lines of particles are evenly spaced, 100  $\mu\text{m}$  apart; we expect the nodes of the standing waves to be distributed evenly horizontally at intervals of half the wavelength of the IDTs. Though not visible in a still image, when water flows through the channel, different particle velocities are observed along the concentrated line, indicating that the particles may focus at multiple heights within the channel. This suggests that two or more nodes are stacked vertically, which is also consistent with nodes formed from waves emitted directly into the water channel.



**Figure 7: 6  $\mu\text{m}$  particles concentrated at the nodes of standing waves in water in a PDMS channel on 128° Y-cut black lithium niobate with a 200  $\mu\text{m}$  wavelength IDT pair driven at a frequency of 19.76 MHz**

PMMA also has reduced attenuation relative to PDMS, and as a result there are multiple paths in addition to the direct path from the lithium niobate substrate to water. Consequently, in PMMA, there exist acoustic nodes in addition to the evenly-spaced half-wavelength nodes seen in PDMS channels. Figure 8 shows 6  $\mu\text{m}$  particles concentrated at such nodes in a PMMA channel on Y-cut, Z-propagating clear lithium niobate. The IDT pair of the device is driven by a sinusoidal signal generated by a National Instruments PXI-5421, 100 MS/s, 16-Bit Arbitrary Waveform Generator and amplified by a NP Technologies Model NP-520 RF amplifier with a linear range of 3-90 MHz and maximum power of 50 watts. The peak to peak voltage of the signal at the IDTs is 17.2 volts and the IDTs are driven at 17.68 MHz. As seen in Figure 8, the lines of concentrated particles are not evenly spaced and are separated across the channel width by less than half of the IDT wavelength. By observing the different velocities of the particle lines with flow through the channel, and by adjusting the focus of the microscope to bring different lines of particles into focus, we can observe that the particles are at various heights within the PMMA channel. PMMA channels display more complex node patterns than PDMS channels, which must be taken into account in device design.

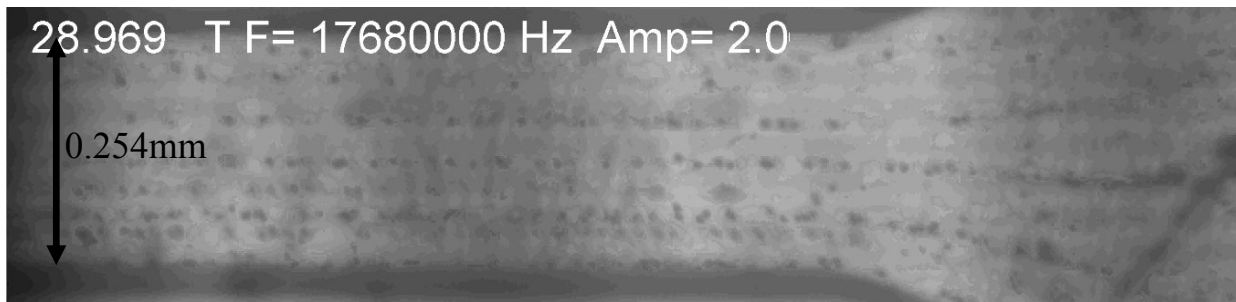


**Figure 8:** 6  $\mu\text{m}$  particles concentrated at nodes in a PMMA channel on Y-cut, Z-propagating clear lithium niobate with a 200  $\mu\text{m}$  wavelength IDT pair driven at a frequency of 17.68 MHz.

## 6. PARTICLE SORTING TECHNIQUES

Because particles of different sizes or density move at different velocities in an acoustic field, it should be possible to separate particles by their properties. We previously attempted to alternate between standing waves and traveling waves to separate particles by driving faster-moving particles toward one side of the channel, thereby separating them from slower moving particles. However, the simplest way to alternate between traveling and standing waves would be to alternately turn off and on one IDT in a pair of IDTs. An un-driven IDT left open circuited acts as a reflector, thus creating standing waves in a pair of IDTs by reflecting the waves back from the other IDT. We expected, in principle, that a shorted IDT would not reflect and might enable waves generated by the driven IDT to travel past it, thus temporarily creating traveling waves instead of standing waves. We tested this hypothesis by flowing particles through both the PMMA channel displayed in Figure 8 and the PDMS channel displayed in Figure 7, and driving one IDT while shorting the other. However, with one IDT shorted (and with damping applied outside of the IDT pair) the particles in continued to form into lines qualitatively similar to Figure 7 and Figure 8, though in slightly different places. This indicated that standing waves were still forming from reflections off of the opposing (shorted) IDT.

We performed COMSOL simulations to explore this question further. In this simulation we drove one IDT on a 0.5-mm thick substrate and performed a 2D frequency domain analysis with the opposing IDT open and then with the same opposing IDT shorted. We then repeated the simulations multiple times while increasing the thickness of the substrate to 1 mm, 2 mm and 4 mm. By taking a line integral of charge over the driven fingers of the driven IDT, we can calculate the conductance of the IDT in the simulations. Figure 9 compares the conductance versus frequency for the 0.5 mm thick simulations and the 4 mm thick simulations. Peaks separated by approximately 130 kHz indicate reflections from the opposing IDT, and the relative amplitude of these peaks indicates the reflectivity of the opposing IDT. The presence of structured peaks in the shorted 0.5 mm thick simulation demonstrates that, despite that fact that the amplitude of the reflection is less than that with an opposing open IDT, the reflection definitely exists, so standing waves will be formed. This means that shorting one IDT is not an effective way to switch from standing waves to traveling waves. The conductance results for all wafer thicknesses above 1 mm were almost identical to one another, indicating that the simulation reached the thickness required for primarily surface waves. The 4-mm thick simulations in Figure 9 show

that, when surface waves dominate, the reflectivity of an opposing open IDT increases significantly, supporting our hypothesis that we do not have primarily surface waves at 0.5 mm, and demonstrating that open IDTs are more effective reflectors of surface waves than bulk waves. The 4-mm thick simulation, however, also demonstrates that the shorted IDT continues to reflect a significant portion of the waves. Therefore, shorting an opposing IDT is not a viable way to switch to traveling waves.

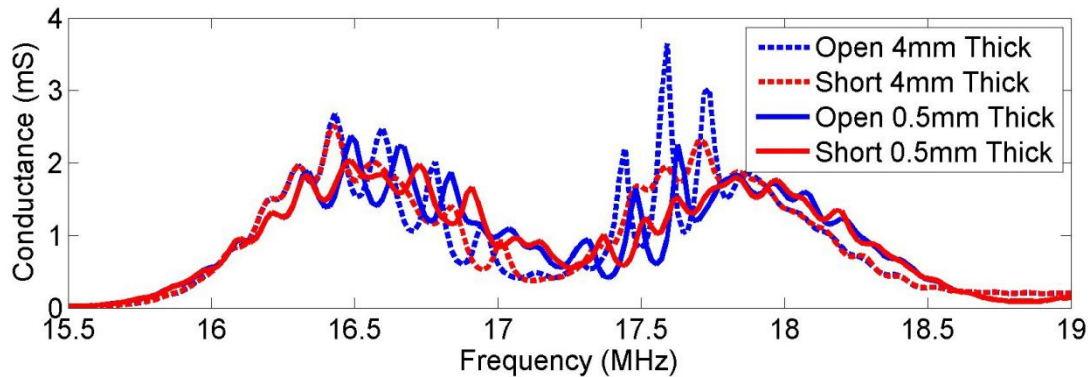


**Figure 9:** Simulated conductance of a 200  $\mu\text{m}$  wavelength IDT on Y-cut, Z-propagating lithium niobate with an opposing IDT either open or shorted, and a substrate thickness of either 0.5 mm or 4 mm.

## 7. SUMMARY AND CONCLUSIONS

We fabricate IDTs on Y-cut, Z-propagating clear lithium niobate wafers. We use CNC micromachining to fabricate PMMA channels, and we have developed a system for bonding these channels to the lithium niobate wafers using an ultraviolet cured epoxy. PDMS channels were used in many earlier applications. However, PMMA channels are more acoustically active and allow for transfer of more acoustic energy into the water in the microfluidic channel. Our experimental evidence also demonstrates that more acoustic nodes form (at irregular intervals) in PMMA than in PDMS.

We also examined the wave types created by IDTs on 0.5 mm thick Y-cut, Z-propagating lithium niobate. At an operating wavelength near 200  $\mu\text{m}$ , the waves display significant through-thickness displacement components. Through simulation and experiment we know that the non-surface wave characteristics of these waves affect the wave interactions with opposing IDTs and with channels bonded to the surface of the substrate.

We have demonstrated that PMMA channels can be used in acoustic devices that concentrate particles. PMMA can be easily machined and has less damping than PDMS, so it may be an attractive channel material for some applications.

## ACKNOWLEDGEMENTS

This material is based upon work supported by the National Science Foundation under Grant No. CMMI-1235145, "Augmented Surface Acoustic Wave Devices for Microbial Cell Separation on Physiological Principles." Any opinions, findings, and conclusions or recommendations expressed in this material are those of the authors and do not necessarily reflect the views of the National Science Foundation, those of the United States Government, or any agency thereof.

## REFERENCES

- [1] Shi, J., Yazdi, S., Lin, S. S., Ding, X., Chiang, I., Sharp, K., and Huang, T. J., "Three-dimensional continuous particle focusing in a microfluidic channel via standing surface acoustic waves (SSAW)," *Lab Chip*: 11, 2319 (2011).

- [2] Oppenheim, Irving J., et al. "Microparticle transport and concentration with surface acoustic waves." SPIE Smart Structures and Materials+ Nondestructive Evaluation and Health Monitoring. International Society for Optics and Photonics, 2013.
- [3] Langelier, Sean M., Leslie Y. Yeo, and James Friend. "UV epoxy bonding for enhanced SAW transmission and microscale acoustofluidic integration." *Lab on a Chip* 12.16 (2012): 2970-2976.
- [4] Nielsen, Andreas H. "Absorbing boundary conditions for seismic analysis in ABAQUS." ABAQUS Users' Conference. 2006.
- [5] Dauson, E., et al. "Reflections and standing waves for particle concentration in microfluidic channels" Ultrasonics Symposium (IUS), 2013 IEEE International. IEEE, 2013.
- [6] Johansson, Linda, et al. "Surface acoustic wave induced particle manipulation in a PDMS channel—principle concepts for continuous flow applications." *Biomedical microdevices* 14.2 (2012): 279-289.